Published in final edited form as:
Anal Chem. 2009 April 1; 81(7): 2618–2625. doi:10.1021/ac802538x.

Multiplexed DNA detection using spectrally encoded porous SiO_2 photonic crystal particles

Shawn O. Meade[a], **Michelle Y. Chen**[b], **Michael J. Sailor**[a,b], and **Gordon M. Miskelly**[c]

[a]Department of Chemistry and Biochemistry, University of California, San Diego, 9500 Gilman Drive, La Jolla, CA 92093-0358 [b]Department of Bioengineering, University of California, San Diego, 9500 Gilman Drive, La Jolla, CA 92093-0358 [c]Department of Chemistry, The University of Auckland, Private Bag 92019, Auckland, New Zealand

Abstract

A particle-based multiplexed DNA assay based on encoded porous SiO_2 photonic crystal disks is demonstrated. A "spectral barcode" is generated by electrochemical etch of a single-crystal silicon wafer using a programmed current-time waveform. A lithographic procedure is used to isolate cylindrical microparticles 25 microns in diameter and 10 microns thick, which are then oxidized, modified with a silane linker, and conjugated to various amino functionalized oligonucleotide probes via cyanuric chloride. It is shown that the particles can be decoded based on their reflectivity spectra, and that a multiple analyte assay can be performed in a single sample with a modified fluorescence microscope. The homogeneity of the reflectivity and fluorescence spectra, both within and across the microparticles is also reported.

Keywords

Encoded photonic crystal; high-throughput screening; multiplexed DNA detection; image analysis; porous silica; porous silicon

Multiplexed genomic assays, used in genotyping, gene expression and epigenomics, play an important role in disease research, leading to new diagnostic and therapeutic tools.[1] Microarray systems can employ spatially segregated chemical probe sites, where the identity of each probe site is defined by a spatial address,[2–4] or they can employ randomly ordered probe supports, which can take the form of microspheres, microrods, or microdiscs.[1, 5, 6] In order to harvest the information from randomly ordered probes, some form of identifier must be incorporated into the microcarrier. Quantum dots,[7, 8] striped metallic rods,[9] fluorescent dyes,[10] photonic crystal beads,[11] and holographic microgratings[12] are examples of materials that have been used as identifiers. This work presents a system based on electrochemically etched porous Si particles,[13–16] in which the identifier consists of a one-dimensional photonic crystal. The photonic crystal is etched directly into the porous nanostructure, which displays a characteristic optical reflectivity spectrum. The process allows the generation over a million distinct codes, referred to as "spectral barcodes" because of their origin in the reflectivity spectrum of the photonic crystal.[13]

In this work, we demonstrate that the photonic crystal particles can be employed in a standard high-throughput screening application—the detection and discrimination of complementary

Correspondence to: Michael J. Sailor; Gordon M. Miskelly.

DNA oligonucleotides. Thermal oxidation of the encoded porous Si particles allows them to be modified using silane coupling chemistries while imparting stability sufficient for the assay conditions. A fluorescence microscope modified with a tunable light source is used to read the photonic codes in the particles. The light source uses a scanning monochromator, which enables the rapid assay of many different codes simultaneously. The photonic encoding method is validated with a DNA binding assay involving two fluorescently labeled oligonucleotide targets in solution and three immobilized probe oligonucleotides, two of which are complementary to the targets.[6]

EXPERIMENTAL SECTION

Oligonucleotide synthesis

Following the work of Kucho et al.,[17] two 50-mer oligonucleotides, P1 and P2, were designed with sequences ACT GTG TGA TGA AGT TTG GTC AGT CGG CTT GTT ATT ATC TCG TGC TTG TA and TCC TGT AAT GAT CCA GGT GAG TGA TAT GCC ATA CAT CCT AGA TCC TTA TA, respectively. Calculations for these sequences using OligoAnalyzer (http://www.ldtdna.com) gave calculated duplex melting temperatures of 85.4 and 83.4 °C, respectively; equilibrium binding free energies of −89.26 and −86.19 kcal/mol, respectively; and a guanine and cytosine (GC) content of 42 and 40 %, respectively. A third sequence, P3, TCT GGA TAG TCA TAC GTC ACC CTC GCT TAG GAT CTA TAC TTA CTA TAC TA, was prepared as a nonspecific binding control. All three probes were modified with 5' amino C6 linkers and supplied in HPLC-purified form (Operon). Two fluorescently-labeled target sequences, T1 and T2, complementary for P1 and P2, respectively, were also obtained from Operon. T1 was labeled with the fluorescent dye Alexa Fluor 555 and T2 was labeled with Alexa Fluor 680. In order to optimize the specificity of this model system, interactions between non-complimentary pairs and hairpins were reduced by designing the interactions to possess binding free energies of −6.78 kcal/mol or smaller. All OligoAnalyzer calculations for melting temperatures and free energies assumed a salt concentration of 1 M, a temperature of 25 °C and an oligonucleotide concentration of 500 nM.

Fabrication of encoded porous Si particles

Encoded porous Si samples were prepared using methods described previously, with minor modifications.[13] A crystalline silicon wafer (resistivity 1 mΩ-cm) was electrochemically etched in an HF solution (3:1 aqueous 49% HF:ethanol by volume) using a current-time waveform consisting of several superimposed sine waves of different frequencies. A layer of Omnicoat (Microchem) was applied to the porous layer, followed by the deposition of aluminum by sputter coating. The substrate was then patterned with SU-8-25 photoresist in the shape of disks 25 μm in diameter. The unmasked porous silicon and aluminum were removed with a chlorine plasma reactive ion etch in 3 steps: (1) argon plasma supplied at a rate of 30 sccm, 100 s at 200 W of RIE power, pressure of 180 mTorr at 25 °C; (2) mixture of Cl_2, BCl_3, and CH_4, supplied at 30, 30, and 3 sccm, respectively, 30 s at 300 W of RIE power, pressure of 180 mTorr at 25 °C; (3) pressure reduced to 15 mTorr, 300 s at 350 W of RIE power at 25 °C. The porous microparticles were then removed with an electropolishing step consisting of a 100 sec current pulse at a current density of 4 mA/cm^2 in 1:14.5 aqueous 49% HF:ethanol. The substrate was wetted with ethanol immediately prior to immersion in the electropolishing electrolyte. The freestanding microfabricated porous Si particles were then converted to silica (SiO_2) by thermal oxidation. The porous Si particles were transferred to a nickel crucible and placed in a tube furnace at 500 °C, ramped to 950 °C at a rate of 50 °C /min, held at 950 °C for 30 min, cooled back to 500 °C and then removed from the furnace. The particles were rinsed in the crucible with 0.05% $HCl_{(aq)}$, transferred by pipette to a microcentrifuge tube and finally washed with absolute ethanol.

Oligonucleotide Immobilization Chemistry

Oligonucleotide probes were attached to the encoded porous silica particles after the method of Steinberg et al. (Figure 1).[18] A 1 mL aliquot of 0.5% 3-aminopropyltriethoxysilane (Aldrich Chemicals, Inc.) in ethanol was added to approximately 10^5 particles and shaken for 1 h. The particles were washed with ethanol three times and once with acetonitrile in a centrifuge filter (Nanosep, 0.2 μm, Pall). Next, acetonitrile (980 μL), N,N-diisopropylethylamine (20 μL, Aldrich Chemicals, Inc.), and cyanuric chloride (10 mg, Aldrich Chemicals, Inc.) were added to the particles and the mixture was allowed to react for 2 h with constant shaking. The particles were then washed with acetonitrile 4 times, suspended in ethanol, and transferred to a microcentrifuge tube. The particles were settled by centrifugation at 4000 RPM and the supernatant decanted to a volume of approximately 25 μL. A 1 mL aliquot of the 50-mer oligonucleotide (500 nM, 5' amino-C6 modified) in 0.05 M sodium borate buffer, 2 M NaCl, at pH 8.5 was added to the particles and shaken overnight. The DNA-modified particles were then washed four times with 0.05 M sodium borate buffer using the centrifugal filter mentioned above.

Oligonucleotide Hybridization

Hybridization was performed using a method based on that reported by Steinberg et al.[18] Three different encoded particle types were prepared as described above. Particle type 1 was functionalized with oligonucleotide sequence P1, particle type 2 with P2, and particle type 3 with P3. The three particle types (consisting of approximately 10^5 particles per type) were pooled together, and suspended in the hybridization buffer (0.1 M potassium phosphate, 1 M sodium chloride, 0.1 % Tween-20, and 5 % ethanol, at a pH of 7.6). The target oligonucleotides T1 and T2 were then added to the hybridization buffer at a concentration of 10 nM each and the suspension was shaken for 1 h. The particles were then washed three times with hybridization buffer and stored at 4 °C in this solution prior to decoding and assay readout.

Particle Assembly

The suspension of pooled, hybridized and washed particles was vacuum filtered with a porous alumina filter (0.2 μm Anodisc, Whatman) to give an assembly of microparticles suitable for image analysis and spectral decoding. A silicone gasket placed on the filter was used to define a 5 mm diameter circular area for analysis. The dry particle assembly on the filter was inserted into the microscope, imaged, and decoded.

Decoding and Assay Instrumentation

Fluorescence images were acquired using a Nikon LV-150 fluorescence microscope. A 100 W mercury arc lamp with the appropriate bandpass filters was used to excite fluorescence. The microscope was modified to allow illumination of the sample stage with narrow-band light generated by a 100 W tungsten filament lamp in combination with a SpectraPro 275 scanning monochromator (Princeton Instruments-Acton, 13 nm spectral bandwidth). Both light sources were coupled to the body of the microscope through the same c-mount opening via a T-mount adapter equipped with an adjustable diverter mirror to switch between sources. In fluorescence mode, standard filter cubes containing the desired dichroic, excitation and emission filters were placed in the optical path. In the "particle decode" mode, a 50/50 mirror was placed in the optical path. A CoolSnap HQ2 (Photometrics) 14 bit, monochromatic camera was used to capture the fluorescence and reflectivity images. Metamorph software (Molecular Devices) was used to control both the camera and the stepper motor of the monochromator, allowing for the generation of spectral image stacks.

Data acquisition and analysis

In a typical experiment, the alumina collection filter containing a dispersion of dry particles was placed on the microscope stage. All images were acquired with a 10× objective with a binning of 2, yielding a 520 × 696 pixel image. Prior to analysis, the image was cropped to 480 × 480 pixels covering an area of about 570 × 570 μm. A fluorescence image of the assembled particles was acquired with the "Cy5.5" filter combination (excitation filter centered at 650 nm, 45 nm bandpass; dichroic filter centered at 680 nm; emission filter centered at 710 nm, 50 nm bandpass) with an exposure time of 2 s to locate the Alexa Fluor 680 labels. A fluorescence image of the Alexa Fluor 555-labels was then acquired with the "Cy3" filter combination (excitation filter centered at 535 nm, 50 nm bandpass, dichroic at 565 nm; emission filter centered at 610 nm, 75 nm bandpass) with an exposure time of 5 ms with a neutral density filter (ND4, or 25 % transmission) in place. The illumination source was then switched from the filtered mercury lamp to the monochromated tungsten filament lamp, and reflectivity images were acquired while the monochromator was scanned from 400 to 725 nm in 1 nm steps. A 15 ms-exposure image was acquired at each step, resulting in a spectral image stack with 326 sequential images.

The image data were analyzed using purpose-built code developed in Matlab (Mathworks). A mask to locate the microparticles was created based on the maximum in the reflectivity spectrum for each pixel. This mask was either applied directly or the microparticle masks were eroded by 1–3 pixels prior to analysis. The pixels associated with the microparticles were classified based on the peaks in their reflectivity spectra (located using the Matlab functions findpeaks (T. O'Haver) or lmax (S. Koptenko), both with appropriate smoothing applied). The criteria used to classify pixels based on the reflectivity spectra included the height of the highest peak above the background, the relative heights of the smaller peaks, and the relative positions of the peaks.

RESULTS AND DISCUSSION

Encoding and Assay Methodology

Figure 2 provides an overview of the system used to determine if hybridization to a target oligonucleotide has occurred and to identify the target. The preparation of encoded porous Si particles and the general principles of the decoding method used in this work have been presented in earlier publications,[13–16] but a brief summary will be presented here. First, the "spectral barcode" is generated by programmed electrochemical etch of a single crystal Si wafer. The etching waveform consists of a superposition of several sine waves, which generates a complex stratified porosity gradient in the direction perpendicular to the surface of the wafer. This porosity gradient acts like a one-dimensional photonic crystal; the spectrum of light reflected from the material consists of a series of sharp peaks that act as the "bits" in the spectral code. Because of the 1D photonic structure, these spectral codes are only observable when the microscope axis is coincident with the gradient direction; therefore cylindrical disks were chosen since they have two large faces that are perpendicular to the gradient and which tend to adhere to the flat Anodisc filter in the optimal orientation. The porous film is lithographically patterned into disks 25 μm in diameter, and the microparticles, each containing the identical code, are removed from the substrate. The microparticles are stabilized and prepared for surface functionalization by thermal oxidation to give translucent microparticles of porous silica. The oxidation step leads to reproducible changes in the positions of the reflectivity peaks of the microparticles. Thus, a reflectivity peak in the range $\lambda = 600 – 800$ nm prior to oxidation shifts to a new position near 0.75λ nm after oxidation, where λ nm is the original peak position.[19] The porous silica microparticles can be functionalized by silanes, which then enables the application of existing, standard biofunctionalization techniques.[18] The functionalized porous

silica microparticles are modified with an oligonucleotide that acts as the capture probe for the assay (Figure 2A).

To perform the multiplexed DNA hybridization assay, a mixture of microparticles with different spectral barcodes and oligonucleotide probes are added to a solution containing the fluorescently labeled oligonucleotide targets. After reaction the particles are rinsed, retained on an alumina filter, and then fluorescence images and the reflectivity image stack are acquired. The fluorescence images indicate which particles have retained a given type of fluorescently labeled oligonucleotide target, and the reflectivity spectrum at each pixel allows the determination of the identity of the particular probe oligonucleotide sequence.

For this work, the method was validated using a set of three encoded particle types. The first particle type exhibited a code consisting of six peaks, represented in binary fashion as 111111 (Figure 2B and Table 1). The second and fourth peaks were deleted in the code for particle type 2, corresponding to 101011, and the third and fifth peaks were deleted in particle type 3, or 110101. Although the code used in this work was 6 bit binary (64 total possible codes), > 10 bits with grayscale encoding has been demonstrated in this system.[15] Using the immobilization chemistry described above, the particle types were functionalized with the oligonucleotide sequences indicated in Table 1. The three particle types were pooled and two fluorescently-labeled target oligonucleotides, containing the complementary sequences to particle types 1 or 2, were incubated with the particles.

The multiplex assay was decoded using a system that consisted of a standard fluorescence microscope combined with a scanning monochromator that provides a spectrally tunable illumination source. While systems capable of both fluorescence detection and spectral microscopy have been constructed and demonstrated previously,[16,20] the present system provided ready access to the narrow bandwidth reflectivity spectra required to decode multi-bit spectral barcodes over an entire field of view. The fluorescence data acquired for an assembly of the microparticles after the multiplex hybridization step are presented as a false color image in Figure 3A. In this image, the particles to which the target oligonucleotides are bound appear as green or red, corresponding to the Alexa Fluor 555 (610 nm) and Alexa Fluor 680 (710 nm) emission channels, respectively. The target oligonucleotides, designated as T1 and T2, consist of a complementary sequence to one of the capture probes and an Alexa Fluor indicator dye label as indicated in Table 1.

Decoding Particles using the Reflectivity Image Stack

The image stack was analyzed with a Matlab program that classified the individual pixels of each image into a group (representing each photonic code) after the work of Mansfield et al.[21] The sharp spectral peaks derived from the porous SiO_2 photonic crystals (Figure 2B) represent bits in a binary code,[15, 16] with each microparticle having only one code, and therefore spectral unmixing methods for pixel classification were not required. Instead, each pixel associated with a microparticle was identified, decoded, and classified in the following sequence:

1. An image was created showing the maximum light intensity at any wavelength in the reflectivity stack for each pixel. This image was then spatially top hat filtered with a disk structuring element slightly larger than the microparticle size, followed by morphological closing of the image with a smaller disk to give a mask identifying the locations of the microparticles. The pixel spectra were then background-corrected to allow for spatial non-uniformity of the illumination. Further masks were created that eroded the microparticle locations by 1–3 pixels.

2. The spectrum of each pixel identified by these masks was scanned for reflectivity maxima above set height and width thresholds, and the wavelength and intensity of each spectral maximum was determined.

3. Each code includes a peak at short wavelength that was used as a reference peak. The location of this first peak in the spectra of all the microparticle-associated pixels that showed at least four spectral peaks was 472 nm with a standard deviation of 13 nm (n= 6356). The location of each subsequent peak in the code was determined relative to this peak, resulting in a set of relative peak position (RPP) values with much greater precision than the absolute peak positions. Thus, the standard deviations for the RPP ranged from 2.0 nm (second peak) to 3.2 nm (fifth and sixth peaks). The distributions of RPP were even less variable if pixels near the edges of the microparticles were discarded, Figure 4.

4. Each pixel was decoded based on the number of reflectivity peaks and the values of each RPP. The RPP and the peak intensities were tested against predetermined acceptance criteria assigned to a particular code. The acceptance criteria consist of three parameters: the number of RPP values expected for the code, the upper and lower wavelength boundaries of each of the expected RPP values and an intensity threshold for each peak in the code. Pixels meeting these criteria were classified into one of the three microparticle code types. If a pixel did not meet all the predetermined criteria, then it was marked as invalid. In addition, most data reported in this paper are derived using masks in which microparticle locations have been eroded by 1 or more pixels. The spectral criteria combined with this spatial filtering were set to ensure there were no false classifications of single pixels based on the classifications of the surrounding pixels in the same microparticle. The spectral and spatial criteria used lead to a large number of pixels that are classified as invalid. However, within each microparticle the majority of pixels are classified correctly.

5. Finally, the photonic codes were compared to the fluorescence result to determine true positive and true negative results. An indexed color image representing the results of the decoding algorithm applied to the reflectivity image stack is shown in Figure 3C. Pixels decoded as 111111, 101011, 110101 are indicated as green, red, and blue, respectively. Pixels that fail the classification routine are assigned a grey value in the image, while background pixels are shown as black. The irregular object near the center of the images in Figure 3 was not associated with a photonic structure, and so pixels in this region have been excluded from the classification analysis.

Figure 5 shows plots of the fluorescence at 610 nm (Alexa Fluor 555) and 710 nm (Alexa Fluor 680) measured for each microparticle-associated pixel, with the data points being coded based on the reflectivity spectrum at each pixel. The data in both plots show separation of the three code types, indicating that the method can correctly identify particle types under the conditions of a fluorescent oligonucleotide assay. The average intensity measured in each fluorescence channel for each particle type, the standard deviation, and the % coefficient of variance for the data are given in Table 2. Pixels decoded as 111111 exhibited fluorescence intensity values that were highest in the Alexa Fluor 555 channel and low in the Alexa Fluor 680 channel (Figure 5). This is in agreement with expected results, because microparticles of code 111111 were functionalized with capture oligonucleotide sequence P1, whose complementary oligonucleotide target probe (T1) was labeled with Alexa Fluor 555 dye (Table 1). The 101011 microparticles were functionalized with capture oligonucleotide sequence P2, whose complementary oligonucleotide target probe (T2) was labeled with Alexa Fluor 680 dye (Table 1). Correspondingly, pixels decoded as 101011 exhibited fluorescence intensity values that were low in the Alexa Fluor 555 channel and highest in the Alexa Fluor 680 channel (Figure 5). Pixels decoded as 110101 exhibited fluorescence intensity values that were low in both fluorescence channels relative to pixels decoded as 111111 or 101011, consistent with their

being functionalized with oligonucleotide P3, for which there was no complementary target sequence in the analyte solution. Because these results match the experimental design, we have demonstrated that the immobilized probes and reflectivity codes are stable through the assay conditions and that the system is capable of detecting multiple analytes in a single sample.

Figure 5 shows that pixels decoded as 110101 and 111111 display fluorescence intensities in the Alexa Fluor 680 channel that are approximately half that of the 101011 particles that were intentionally labeled with Alexa Fluor 680, while pixels decoded as 101011 and 111111 display fluorescence intensities in the Alexa Fluor 555 channel that are approximately one tenth of the 110101 particles that were intentionally labeled with Alexa Fluor 555. The relatively long exposure time required to acquire data for the Alexa Fluor 680 channel suggests that background fluorescence or bleed through of the Alexa Fluor 555 fluorescence might be contributing to the observed results. However, the “true” background pixels (in regions corresponding to the Anodisc filter) displayed very low levels of fluorescence in both channels, and the irregular object near the center of image 4B only displays fluorescence in the Alexa Fluor 555 and not the Alexa Fluor 680 channel. Thus the data suggest that some Alexa Fluor 680 dye has crossed over to the Alexa Fluor 555-labeled particles during the experiment, presumably due to inefficient coupling chemistry.

The separation between the fluorescence intensities of the pixels corresponding to the 111111/110101 and 101011/110101 codes demonstrates that the assay exhibited low nonspecific binding. There is a slight overlap of the Alexa Fluor 680 fluorescence for the 101011 and 110101 pixels represented in Figure 5A, with nine datapoints from the 101011 code displaying lower fluorescence intensity than the most intense 110101 code datapoint. This plot was prepared from data obtained after 1 pixel erosion around the edges of each microparticle. Erosion of the microparticles by 2 or 3 pixels leads to a decrease in this overlap in fluorescence intensities to 1 and 0 datapoints respectively.

Microparticle shape effects

The porous SiO_2 microparticles used in this work are 1-dimensional photonic crystals. The layers that comprise the photonic crystal exist in layers parallel to the flat face of the disk-shaped particle. The photonic spectrum is only observable when the microscope axis is perpendicular to these flat faces; thus if a particle is lying on edge it cannot be decoded. As can be seen in Figures 3A and 3B, not all the particles are positioned with their flat faces aligned with the optical axis. Some of the microparticles that appear either red or green in the fluorescence image of Figure 3A appear faint in the reflectivity image of Figure 3B and black in the images of Figures 3C and 3D. The particles that are lying on their edges do not reflect light strongly, and they do not display a spectrum corresponding to one of the reflectivity codes. These particles are therefore rejected by the decoding algorithm. Although the majority of particles tend to lie on the sampling substrate in the correct orientation due to their cylindrical disk shape, the geometric dependence of the reflectivity spectrum poses a limitation to the yield and overall throughput of the method.

The variability of datapoints corresponding to the code 111111 (along the AF 555 axis) was quite high (Figure 5) with a coefficient of variation of 34% for Figure 5A. In fact, the distribution appears to be bimodal. This is not due to edge effects, even though the fluorescence appears brighter at the edges of particles in Figure 3A, since pixels corresponding to the edges are removed by spatial and spectral filtering (see below). The more likely explanation is that the microparticles are not exactly symmetric, with the preparation leading to different surfaces on the top and bottom of the particles. The SEM micrograph in Figure 6 shows two microparticles: the one on the left is oriented in the way it was prepared, while the one on the right is upside down. The face presented by the upside down particle reveals roughness that is characteristic of the morphology produced when the porous Si/substrate Si interface is ruptured

by the lift-off etching step. We postulate that the two populations of fluorescence intensity are associated with the differing morphologies of these faces. The fluorescence data obtained at 710 nm, corresponding to the seven microparticles containing the 110101 code, do not show such a clear separation, although the distribution displays a shoulder with intensity of ~5000 compared to the main intensity of 6000–6500. This shoulder is primarily associated with pixels on one of the seven microparticles identified as 110101.

The ability to direct the orientation of porous Si particles by specific surface chemical interactions has been demonstrated, and so it is possible that the microparticle shape limitations discussed above could be overcome.[22]

Edge effects

Many pixels at the edges of the microparticles were distinguishable from pixels in the centers of microparticles in both the fluorescence and reflectivity images. In the fluorescence image, Figure 3A, several microparticles (especially the brighter green ones) show increased fluorescence intensity at their periphery. This could be due to wave-guiding effects within the microparticle or to an increased concentration of fluorescent label near the surface of the microparticle. Pixels near the edges also display different reflectivity spectra; the spectra typically are blue-shifted slightly in comparison to spectra of pixels near the center. Edge pixels also often display less well-defined reflectivity spectra. There is an increase in molar volume upon oxidation of porous silicon to silica,[23] so some of these edge effects may be due to the differing amount of expansion upon oxidation that occurs at the microparticle edges compared to the more constrained center. The spectral irregularities resulted in rejection of many edge pixels by the algorithm developed in this study, and if the criteria were made less stringent some edge pixels were misclassified. For these reasons we investigated the effect of spatial filtering to remove these pixels from the analysis.

Figure 3D shows the pixels that were not placed into one of the three classes when a spatial edge mask is applied. It is evident that many pixels at the edges of microparticles are not classified correctly. Indeed, in this particular instance one pixel at the edge of a microparticle that should have been a member of class 111111 was misclassified as 101011. Erosion of the microparticle images by 1 to 3 pixels (corresponding to 1.2 – 3.6 μm, compared to their diameter of 25 μm) reduced the number of invalid (non-classified) pixels, at the cost of slightly decreased numbers of correctly identified pixels, Figure 7. This spatial filtering also improves the separation of the fluorescence intensities associated with each microparticle type, as shown in Figure 5B (3 pixel erosion) compared to Figure 5A (1 pixel erosion).

CONCLUSIONS

This work demonstrated a system that is capable of detecting multiple analytes contained in a single sample using spectrally encoded porous SiO_2 microparticles. The microparticles can be functionalized using silane chemistry and they are stable under biological assay conditions. The photonic codes are identified by analysis of their wavelength-dependant reflectance properties, obtained simultaneously on an ensemble of particles by wavelength-resolved digital imaging. The codes are retained through the preparation and analysis process.

Two target oligonucleotides were conjugated with fluorescent dyes of different colors to provide an independent test of the classifications based on the photonic codes. In practice, a single dye could be used for all sequences because sequence identification is obtained from the reflectivity spectrum of the microparticle to which the sequence is attached. Thus, whether or not a microparticle has probe oligonucleotides complementary to the target oligonucleotide sequences is determined by observing which particles in the ensemble are fluorescent; the identity of the oligonucleotide on each of the fluorescent microparticles is then determined by

decoding the reflectivity spectrum of that microparticle. The method could also be applied to proteomics assays using appropriately tagged fluorescent antibodies or other markers.

The decoding method used in this study is based on proven techniques to classify the spectral characteristics of multiple objects within the field of view of a digital imager.[21, 24] Therefore, analysis using the encoded microparticles described in this work could readily be automated using existing image analysis approaches for massively parallel, high throughput bioassays.

Supplementary Material

Refer to Web version on PubMed Central for supplementary material.

ACKNOWLEDGEMENTS

This material is based upon work supported by the National Cancer Institute of the National Institute of Health (NIH) under grant U54 CA 119335, and by the National Science Foundation under Grant No. DMR-0806859. MJS is a member of the Moores UCSD Cancer Center and the UCSD NanoTUMOR Center.

REFERENCES

1. Fan JB, Chee MS, Gunderson KL. Highly parallel genomic assays. Nat. Rev. Genet 2006;7(8):632–644. [PubMed: 16847463]
2. Chee M, Yang R, Hubbell E, Berno A, Huang XC, Stern D, Winkler J, Lockhart DJ, Morris MS, Fodor SPA. Accessing genetic information with high-density DNA arrays. Science 1996;274:610–614. [PubMed: 8849452]
3. Fodor SPA, Read JL, Pirrung MC, Stryer L, Lu AT, Solas D. Light-Directed, Spatially Addressable Parallel Chemical Synthesis. Science 1999;251(4995):767–773. [PubMed: 1990438]
4. Heller MJ. An active microelectronics device for multiplex DNA analysis. IEEE Engineering in Med. and Bio 1996;15(2):100–104.
5. Ferguson JA, Steemers FJ, Walt DR. High-Density Fiber-Optic DNA Random Microsphere Array. Anal. Chem 2000;72(22):5618–5624. [PubMed: 11101240]
6. Gunderson KL, Kruglyak S, Graige MS, Garcia F, Kermani BG, Zhao C, Che D, Dickinson T, Wickham E, Bierle J, Doucet D, Milewski M, Yang R, Siegmund C, Haas J, Zhou L, Oliphant A, Fan J-B, Barnard S, Chee MS. Decoding Randomly Ordered DNA Arrays. Genome Res 2004;14:870–877. [PubMed: 15078854]
7. Bruchez M, Moronne M, Gin P, Weiss S, Alivisatos AP. Semiconductor nanocrystals as fluorescent biological labels. Science 1998;281(5385):2013–2016. [PubMed: 9748157]
8. Chan WCW, Nie S. Quantum dot bioconjugates for ultrasensitive nonisotopic detection. Science 1998;281:2016–2018. [PubMed: 9748158]
9. Nicewarner-Peña SR, Freeman RG, Reiss BD, He L, Peña DJ, Walton ID, Cromer R, Keating CD, Natan MJ. Submicrometer metallic barcodes. Science 2001;294(5540):137–141. [PubMed: 11588257]
10. Fenniri H, Ding L, Ribbe AE, Zyrianov Y. Barcoded resins: a new concept for polymer-supported combinatorial library self-deconvolution. J. Am. Chem. Soc 2001;123(33):8151–8152. [PubMed: 11506586]
11. Zhao Y, Zhao X, Sun C, Li J, Zhu R, Gu Z. Encoded silica colloidal crystal beads as supports for potential multiplex immunoassay. Anal. Chem 2008;80:1598–1605. [PubMed: 18247635]
12. Moon JA, Putnam MA, Perbost M, Quinn JJ, Trounstine M. Diffraction Grating-Based Encoded Articles for Multiplexed Experiments. US Patent Application 2005/0227252. 2005 October 13;
13. Meade SO, Sailor MJ. Microfabrication of freestanding porous silicon particles containing spectral barcodes. Phys. Status Solidi-Rapid Res. Lett 2007;1(2):R71–R73.
14. Sailor MJ, Link JR. Smart Dust: nanostructured devices in a grain of sand. Chem. Commun 2005:1375–1383.
15. Meade SO, Yoon MS, Ahn KH, Sailor MJ. Porous silicon photonic crystals as encoded microcarriers. Adv. Mater 2004;16(20):1811–1814.

16. Cunin F, Schmedake TA, Link JR, Li YY, Koh J, Bhatia SN, Sailor MJ. Biomolecular screening with encoded porous silicon photonic crystals. Nature Mater 2002;1:39–41. [PubMed: 12618846]

17. Kucho K, Yoneda H, Harada M, Ishiura M. Deterinants of Sensitivity and Specificity in Spotted DNA Microarrays with Unmodified Oligonucleotides. Genes Genet. Syst 2004;79(4):189–197. [PubMed: 15514438]

18. Steinberg G, Stromsborg K, Thomas L, Barker D, Zhao C. Strategies for covalent attachment of DNA to beads. Biopolymers 2004;73:597–605. [PubMed: 15048783]

19. Meade, SO. PhD. San Diego, La Jolla: University of California; 2008. Development of a DNA multiplexing system utilizing encoded porous silica photonic crystal particles.

20. Empedocles SA, Watson AR. Two-dimensional spectral imaging system. US Patent 6759235. 2004

21. Mansfield JR, Gossage KW, Hoyt CC, Levenson RM. Autofluorescence removal, multiplexing, and automated analysis methods for in-vivo fluorescence imaging. J. Biomed. Opt 2005;10(4):041207-1–041207-9.

22. Link JR, Sailor MJ. Smart Dust: Self-assembling, self-orienting photonic crystals of porous Si. Proc. Nat. Acad. Sci 2003;100(19):10607–10610. [PubMed: 12947036]

23. Pap AE, Kordas K, Toth G, Levoska J, Uusimaki A, Vahakangas J, Leppavuori S, George TF. Thermal oxidation of porous silicon: Study on structure. Appl. Phys. Lett 2005;86(4)

24. Dickinson ME, Bearman G, TIlle S, Lansford R, Fraser SE. Multi-spectral imaging and linear unmixing add a whole new dimension to laser scanning fluorescence microscopy. Biotechniques 2001;31(6):1272–1278. [PubMed: 11768655]

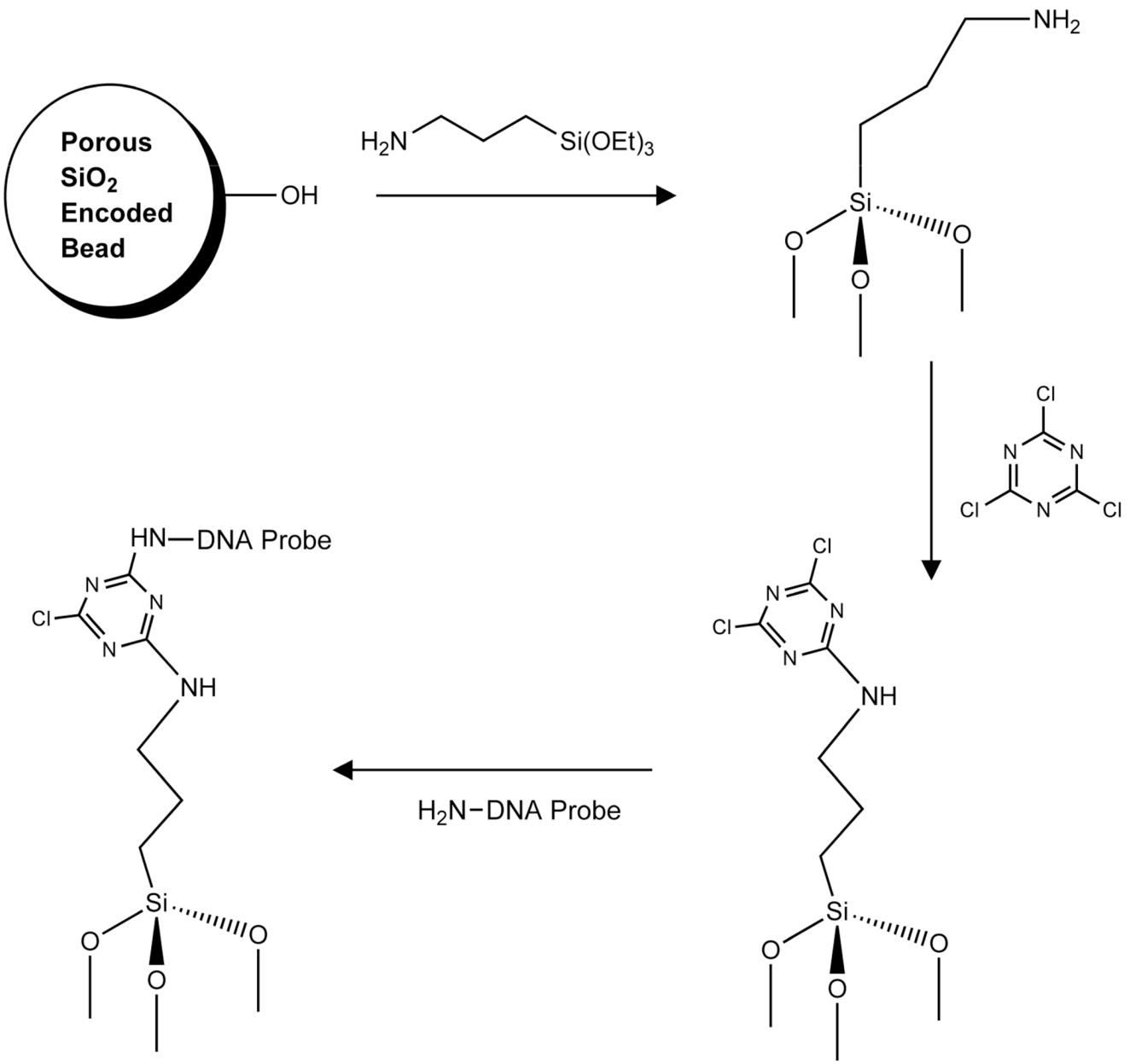

Figure 1. Immobilization chemistry used in this work

(1) The porous silica particles were rinsed in 0.05% HCl (aq) then reacted with 0.5% of 3-aminopropyltriethoxysilane in ethanol for 1h, (2) followed by suspension in acetonitrile and cyanuric chloride activation in the presence of N,N-diisopropylethylamine for 2h. (3) Amino-C6-oligonucleotide probes were allowed to react with the particles overnight.

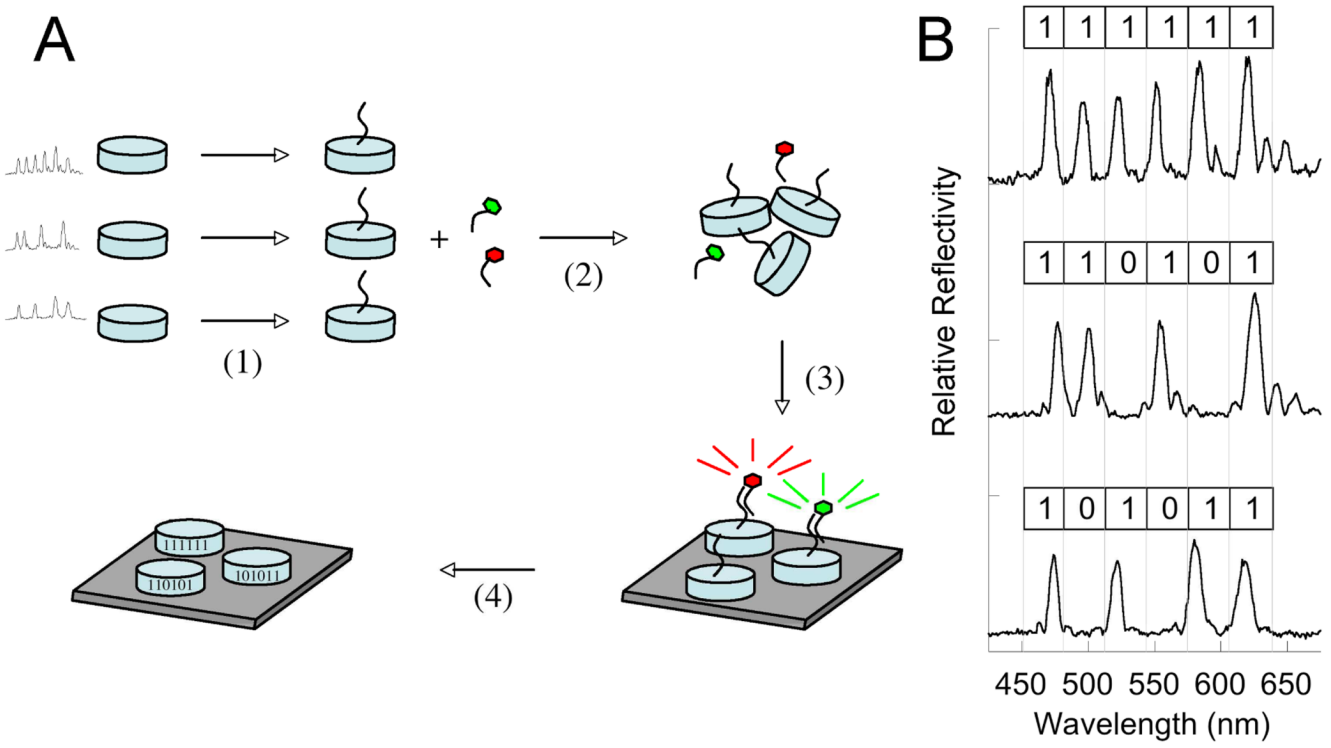

Figure 2.

A. Summary of the procedure used in the DNA hybridization assay. (1) Several types of DNA-labeled encoded particles are prepared. Each set of particles contains a unique spectral barcode (three examples are shown in Figure 2B) and a specific DNA probe sequence. (2) The particle types are pooled together and the combined mixture is reacted with fluorescently labeled target sequences. (3) The particle suspension is washed, assembled onto a surface, and a fluorescence microscope image is acquired. (4) Without moving the particle assembly relative to the imager, reflectivity spectra of all the particles in the field are acquired simultaneously by means of a wavelength-scanned illumination source. **B.** Reflectivity spectra observed for single pixels of each of the three encoded particle types used in this study. The binary codes assigned to each spectrum are shown. To assign the codes, the spectrum is binned into six spectral regions. A bin is assigned a code of “1” if the spectral intensity in that bin exceeds a threshold value. If no peak is observed in the spectral region, the bin is assigned a code of “0.”

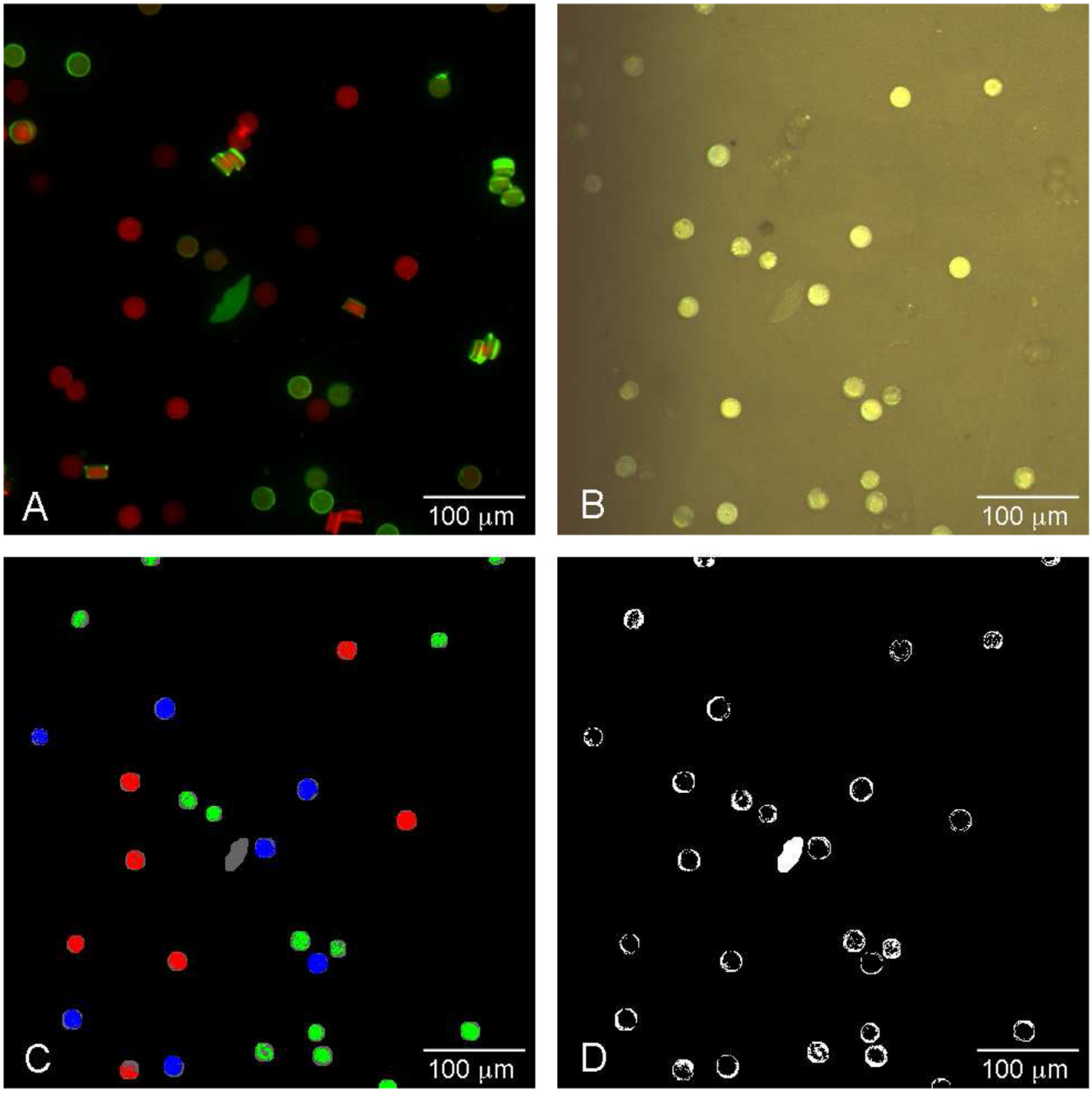

Figure 3.

Microscope images of particle ensembles showing results of fluorescence and reflectivity assays. (**A**) False color image of fluorescence measured from particle ensemble. The green and red colors represent the fluorescence intensity measured in the AF555 channel (Alexa Fluor 555, λ_{em} = 610 nm) and the AF680 channel (Alexa Fluor 680, λ_{em} = 710 nm) respectively. (**B**) Color reflectivity image constructed from the reflectivity image stack. (**C**) Indexed color image resulting from a decode of the reflectivity image stack after 1 pixel morphological erosion of the microparticle locations. Pixels decoded as 111111, 110101, and 101011 are represented as green, blue, and red, respectively. Pixels in the image that fail the decode algorithm are assigned to gray, while background pixels are black. (**D**) Image showing the

positions of pixels that failed the decode algorithm when no morphological erosion is applied to the microparticles. Scale bar is 100 μm.

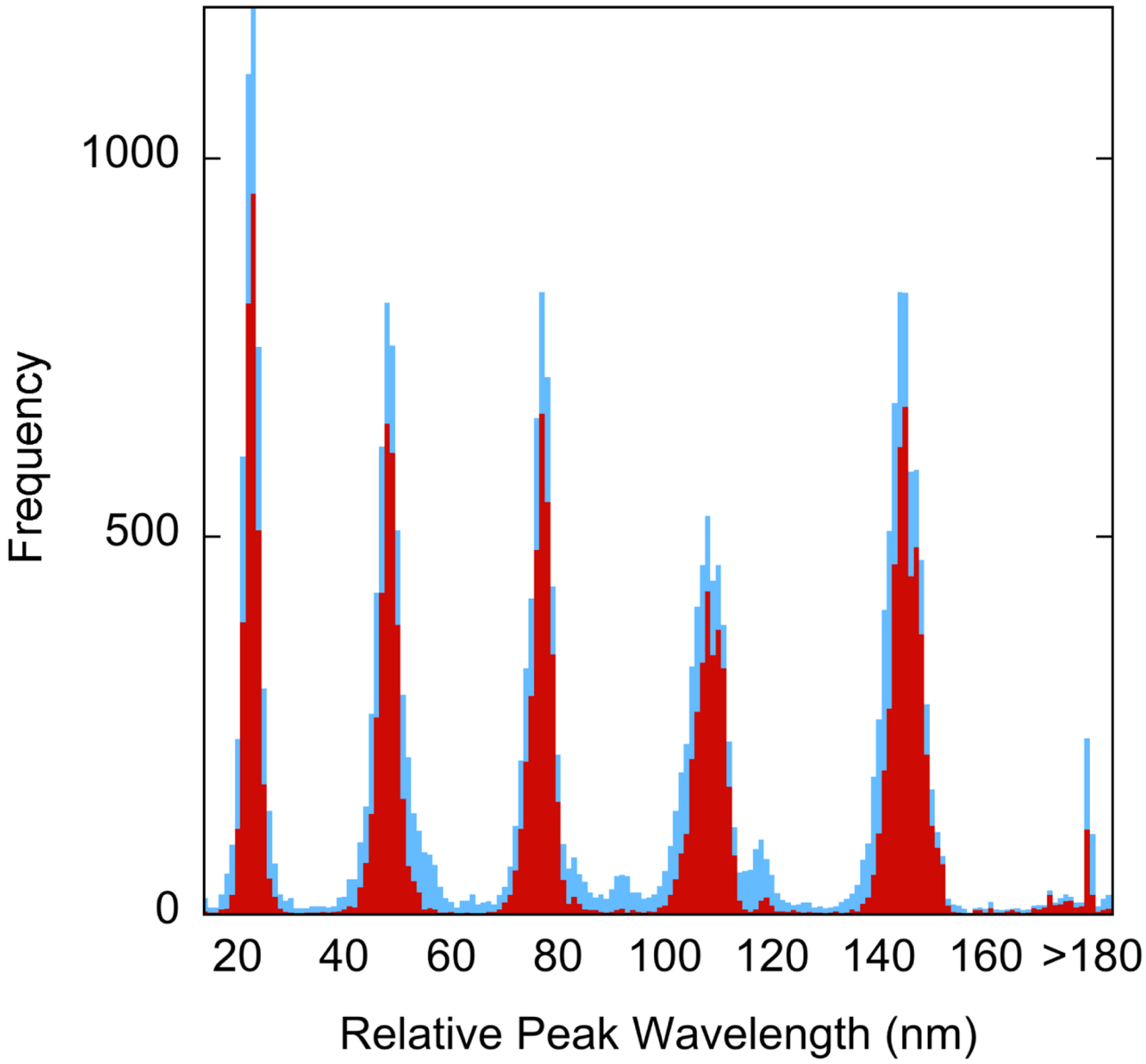

Figure 4.
Distributions of the relative peak positions (RPP) for all pixels identified as belonging to the microparticles with no erosion (blue) and 3 pixel erosion (red) of the microparticle locations.

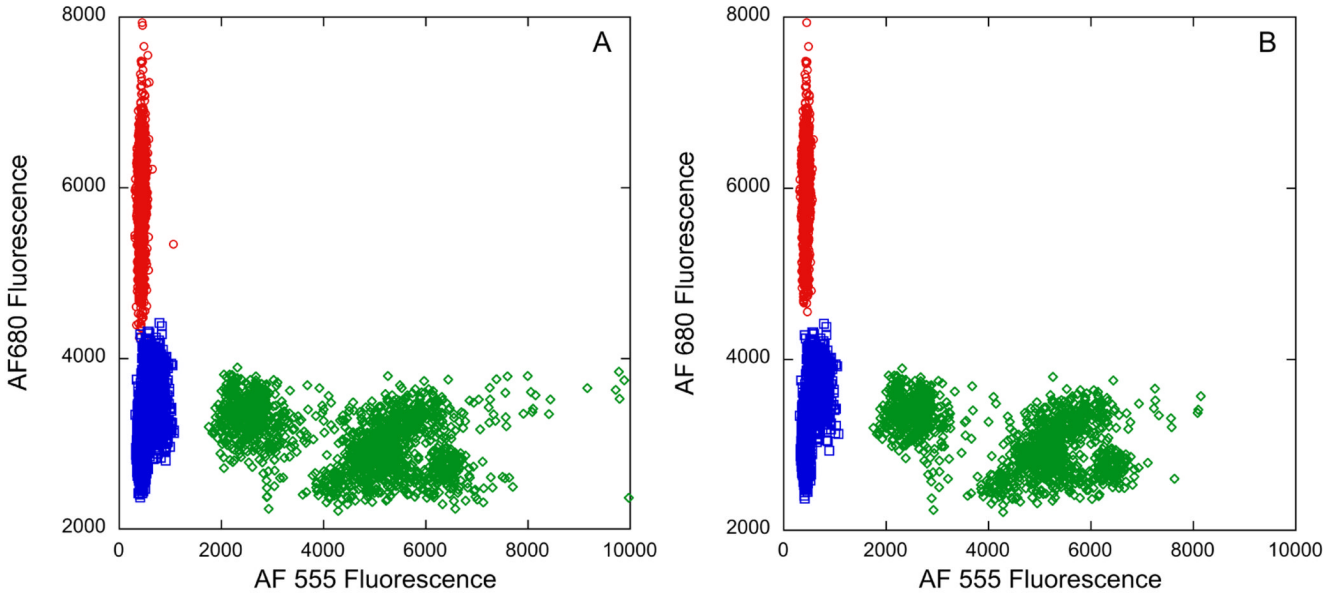

Figure 5.

Scatter plots depicting the classification capability of the spectral decoding algorithm for microparticles that have had (A) 1 pixel eroded from their image edges and (B) 3 pixels eroded from their image edges. The fluorescence intensity measured in the AF680 channel (Alexa Fluor 680, λ_{em} = 710 nm) is plotted against the fluorescence intensity measured in the AF555 channel (Alexa Fluor 555, λ_{em} = 610 nm) for each pixel in the image of Figure 3A corresponding to a classified pixel. The data are represented with red circles, green diamonds, or blue square symbols for codes 101011, 111111, or 110101, respectively (see Table 1). The pixels decoded as 101011, 111111, or 110101 are distributed over 7, 13, and 7 individual particles, respectively.

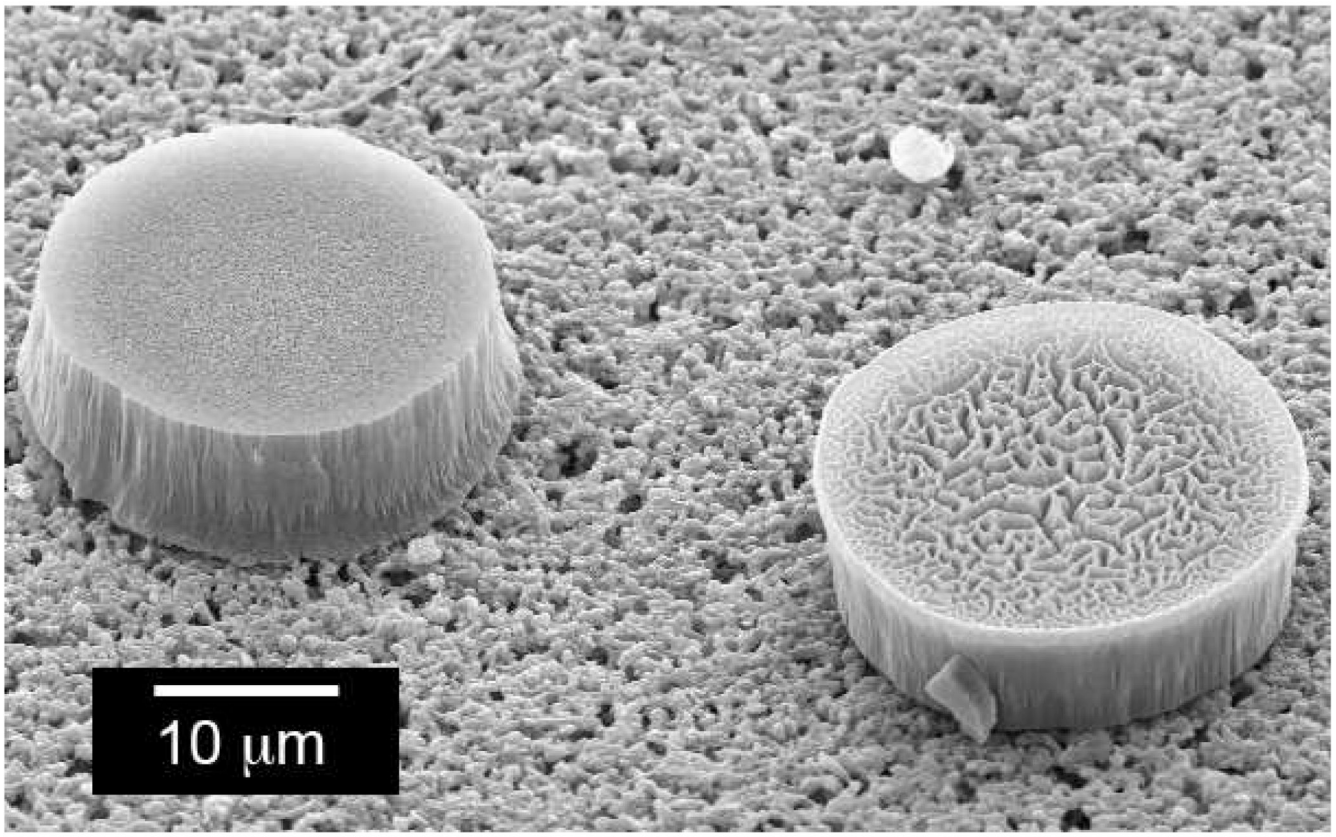

Figure 6.
Scanning electron micrograph showing two porous silicon microparticles on a filter support, showing the different morphologies of the upper and lower surfaces. The surface shown on the particle on the right was at the interface between the particle and the silicon substrate, and it illustrates the pitting generated by the electrochemical liftoff procedure.

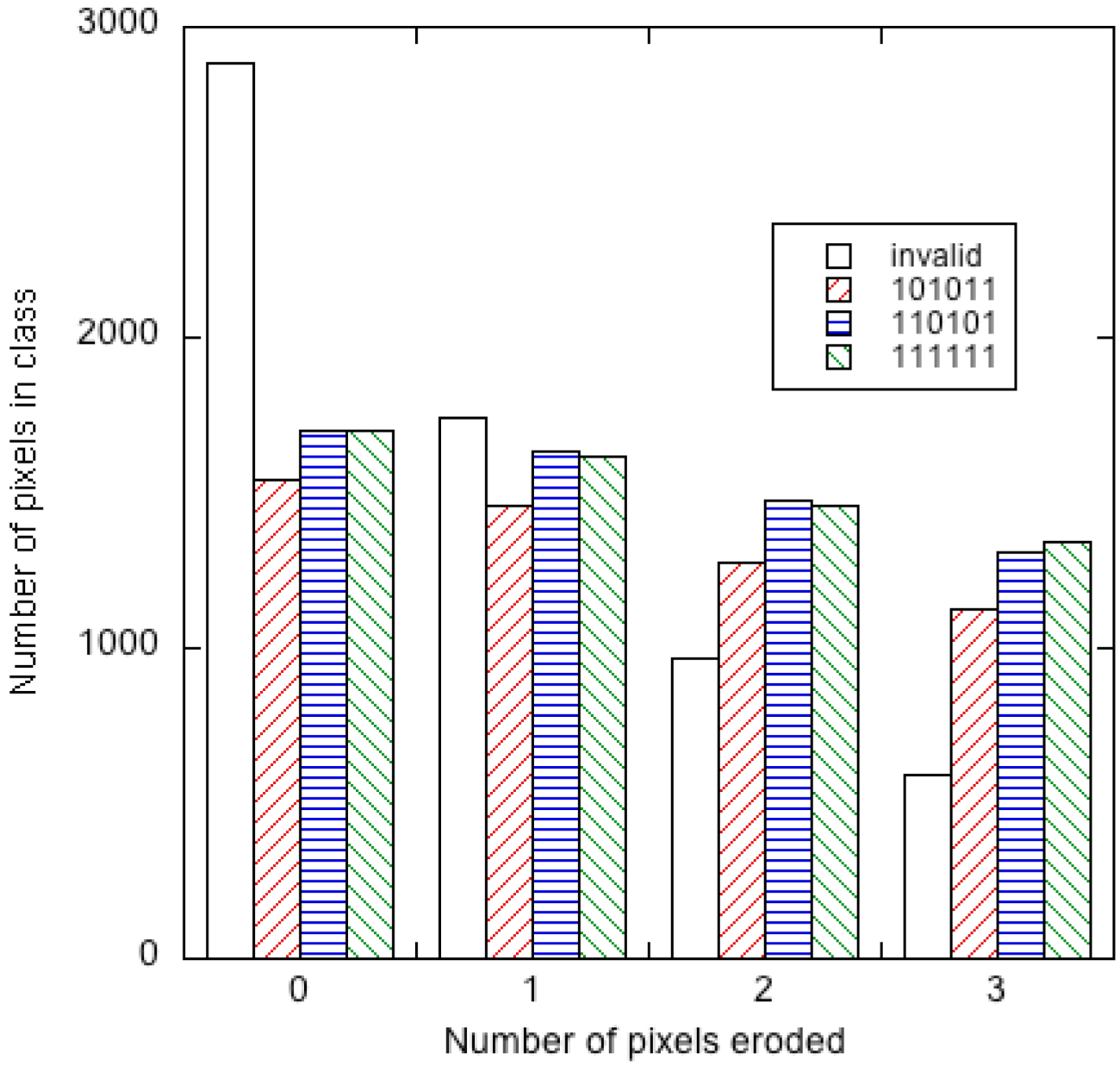

Figure 7.
Figure showing the numbers of pixels classified as 111111, 110101, 101011, and invalid as a function of the number of pixels eroded from the edges of the image of each microparticle.

Table 1

Photonic codes, oligonucleotide sequences, and the corresponding fluorescent label associated with the three particle types used in this work.

Photonic Code	Capture Probe Sequence (Amino C6-5'--3')	Target	Target Label[a]
111111	ACTGTGTGATGAAGTTTGGTCAGTCGGCTTGTTATTATCTCGTGCTTGTA	T1	AF 555
101011	TCCTGTAATGATCCAGGTGAGTGATATGCCATACATCCTAGATCCTTATA	T2	AF 680
110101	TCTGGATAGTCATACGTCACCCTCGCTTAGGATCTATACTTACTATACTA	—	—

[a] AF = Alexa Fluor; indicates the identity of the fluorescent dye attached to the target sequence (T1 or T2) that is complementary to the capture probe sequence indicated. The symbol " – " indicates that no target sequence was used; the capture probe for this particle type was included as a negative (non-specific binding) control for the other target sequences.

TABLE 2

Average pixel intensities from each fluorescence channel for codes represented in Figure 5A.

Code	Channel	Intensity [a]	Stdv	% CV	Number of pixels
111111	AF555	4475	1550	35	1619
111111	AF680	3068	360	12	
101011	AF555	448	44	9.8	1457
101011	AF680	5876	560	9.6	
110101	AF555	547	160	30	1637
110101	AF680	3230	440	14	

[a] 14-bit scale, maximum value 16383